8

Contact Formation on Silicon Carbide by Use of Nickel and Tantalum from a Materials Science Point of View

Yu Cao and Lars Nyborg
Department of Materials and Manufacturing Technology,
Chalmers University of Technology
SE-41296 Gothenburg, Sweden

1. Introduction

The advantageous electrical, thermal and mechanical properties make silicon carbide (SiC) a promising semiconductor for high temperature, high power and high frequency applications. Nickel (Ni) and tantalum (Ta) can be used to form both ohmic and Schottky contact. Since metallization represents one of the most important steps in the fabrication of electronic devices, the knowledge of the interaction between Ni, Ta and SiC are of primary importance for understanding and optimising the device performance.

In this chapter, an introduction of thermodynamics in Ni (or Ta)-Si-C system will be given. The reaction process and mechanisms of Ni-SiC during annealing will be reviewed. The phases existing in the film or at the interface and the distribution of elements in-depth will be clarified. The impact of pre-treatment on SiC substrate and Ni layer thickness on phase distribution will be summarized. The nature of the thermally induced solid-state reactions between Ta or Ni/Ta bilayer and SiC substrate over a wide temperature range will also be discussed.

2. Ni-SiC

2.1 Ni silicides

Nickel silicides play a significant role in the modern electronic device technology (Colgan et al., 1996; Gambino & Colgan, 1998; M. d'Heurle & Zhang, 2007), the reasons being their chemical and thermal stability as well as low electric resistivity. Among all the silicides, NiSi has the lowest specific resistivity (10.5-18 μΩ cm) which is close to that of Ni metal (7-10 μΩ cm) (Lavoie et al., 2004). The next lowest ones are those of Ni_2Si (24-30 μΩ cm) and $NiSi_2$ (34-50 μΩ cm), respectively. The Ni rich silicides have the highest specific resistivity which is 80-90 μΩ cm for Ni_3Si and 90-150 μΩ cm for $Ni_{31}Si_{12}$, respectively. Nickel silicides are also attractive candidates as coating materials for protection of Ni-base superalloys and stainless steel (Lou et al., 2006; Lu & Wang, 2004) because of their excellent combination of wear, corrosion and oxidation resistance.

The Ni-Si equilibrium phase diagram (Nash & Nash, 1992) predicts six stable intermetallic compounds: Ni_3Si, $Ni_{31}Si_{12}$, Ni_2Si, Ni_3Si_2, NiSi and $NiSi_2$. Only three of compounds melt congruently namely $Ni_{31}Si_{12}$, Ni_2Si and NiSi. The others form via the peritectic reaction. The synthesis method of the nickel silicides in Ni-Si system includes conventional melting and casting and solid state reaction between Ni and Si, the latter of which has been realised in two different ways; thin films and bulk diffusion couples. Other techniques such as ion beam mixing (Hsu & Liang, 2005) and mechanical alloying (Lee et al., 2001) can also be used. In the case of thin film reactions, (Ottaviani, 1979; Zheng et al, 1983; Chen et al, 1985; Lee et al, 2000; Yoon et al, 2003), the formation of the compounds depends on the relative amounts of the Ni and Si available for the reactions, the annealing temperature, the atmosphere, and impurities contained in the layers. Important characteristics include sequential appearance of phases, i.e. one compound is formed first and the second starts to form later on, and the absence of certain phases. Ni_2Si is always the first phase to form and Ni_3Si_2 is always absent in thin film experiments. After one of the elements is consumed, the next compound is richer in the remaining element.

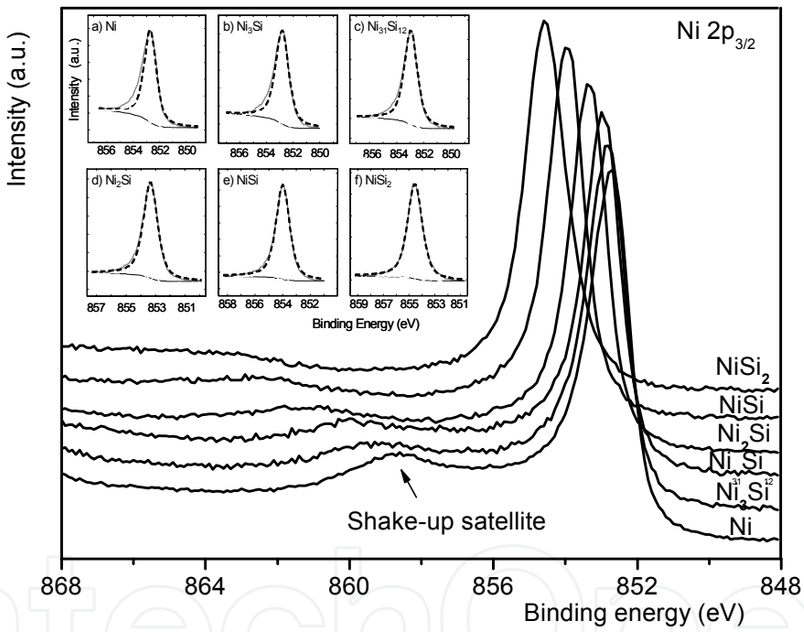

Fig. 1. Normalized XPS core level spectra from different silicides. Surface silicides were prepared by means of thin film solid-state reactions controlling the heating procedure in vacuum and the right sample preparation. (Cao et al., 2009)

XPS (X-ray photoelectron spectroscopy) can be used as a fingerprint for correct phase identification at the surface. The XPS core level spectra of Ni $2p_{3/2}$ in different silicides are shown in Fig. 1. In comparison to the Ni $2p_{3/2}$ peak (852.7 eV) representing the metal, the core level shift ΔEc are 0.1 eV for Ni_3Si, 0.3 eV for $Ni_{31}Si_{12}$, 0.7 eV for Ni_2Si, 1.2 eV for NiSi and 1.9 eV for $NiSi_2$, respectively. With higher amount of Si in the silicides, higher binding energy position and more symmetrical line shape (see insert in Fig. 1) are obtained. The shakeup satellite is shifted to higher binding energy upon increasing Si content as well.

Meanwhile, this structure is weaker and is actually smeared out over a larger binding energy region in the spectrum in the case of $NiSi_2$.

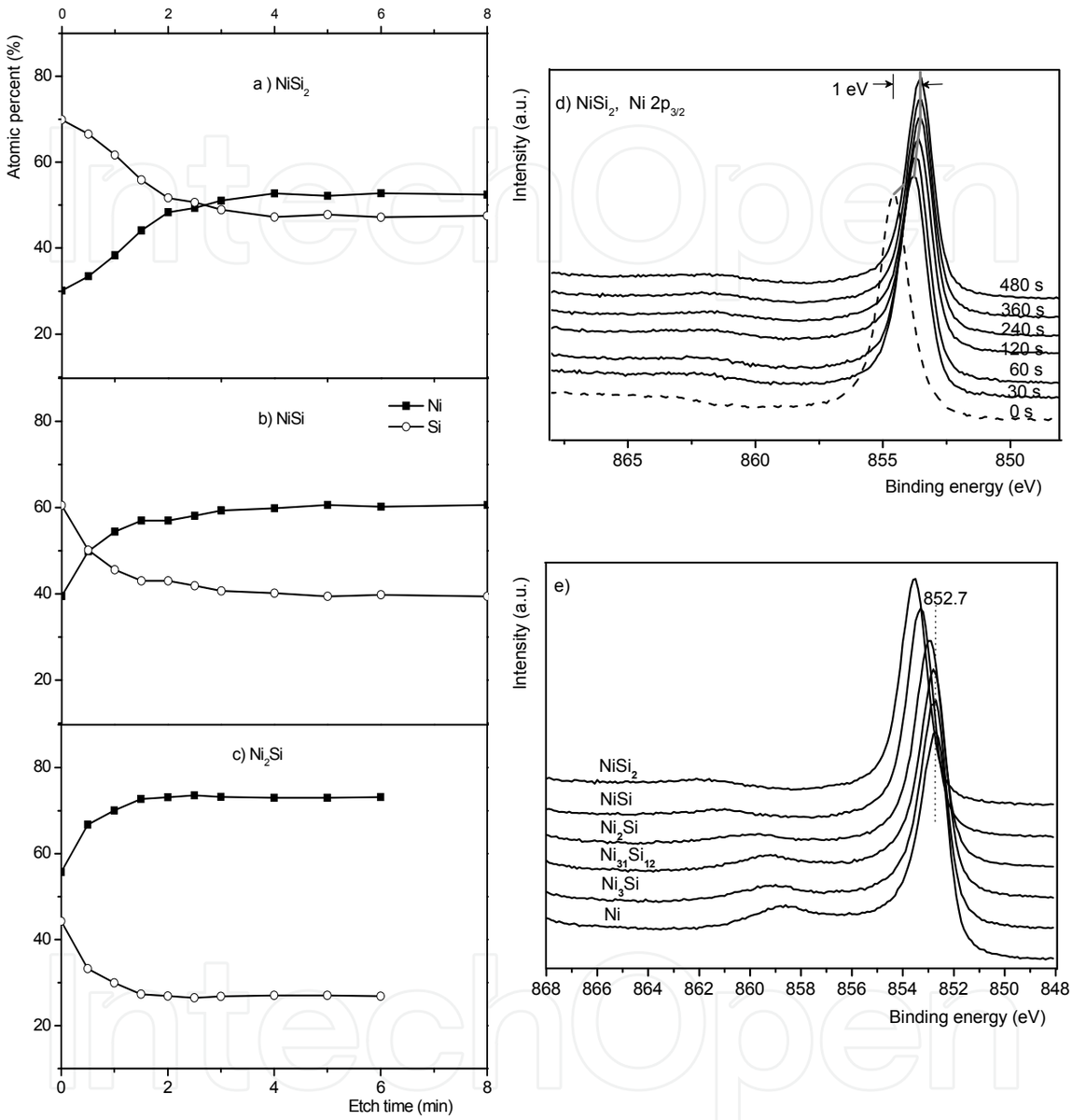

Fig. 2. Depth profiles of a) $NiSi_2$; b) NiSi and c) Ni_2Si derived from successive ion etchings and analysis of the Si 2p and Ni $2p_{3/2}$ levels in XPS. The content of C, O and Si from the surface contamination is not shown here. d) Evolution of XPS Ni $2p_{3/2}$ peaks in $NiSi_2$ during the process of argon ion etching. The spectra are normalized. e) Comparison of normalized Ni $2p_{3/2}$ peaks after 6 min argon ion etching in different silicides. The etch rate calibrated on Ta_2O_5 under these conditions is 4.7 nm /min. Ar ion beam energies of 4 keV are used.

Depth profiling by argon ion etching is a widespread method in studies of film structure and composition. Argon ion etching is a collisional process involving particle-solid

interactions. It induces structural and chemical rearrangement for all the silicides at the surface. Figure 2 a)-c) shows the apparent atomic concentrations of Ni and Si in the silicides vs. etch time (Cao et al., 2009) derived from successive ion etchings and analysis of the Si 2p and Ni $2p_{3/2}$ levels in XPS. During the initial time period of argon ion etching, the surface composition for all the Ni silicides changes with increasing etching time; preferential sputtering of Si occurs, resulting in enrichment of the heavier element Ni. The effect of preferential sputtering decreases with increasing ion beam energy (Cao & Nyborg, 2006). After the prolonged ion etching, the Ni level becomes constant and reaches saturation level (Cao et al., 2009). The smallest preferential sputtering of Si occurs for Ni_3Si, whereas it is most evident for $NiSi_2$. Clearly, the preferential sputtering effect increases with increasing Si content. Moreover, during the process of argon ion etching, all the Ni $2p_{3/2}$ XPS peaks from silicides are moved to a lower binding energy positions until the steady state is reached. For $NiSi_2$, the Ni $2p_{3/2}$ peak is moved downwards in binding energy as much as 1 eV compared to that of the peak without argon ion etching, as shown in Fig. 2d). The corresponding values for NiSi, Ni_2Si and $Ni_{31}Si_{12}$ are 0.6, 0.4 and 0.2 eV, respectively. The steady state position of Ni $2p_{3/2}$ peak for ion etched Ni_3Si is also shifted downwards slightly. Therefore, not only the surface composition is changed with the ion etching, but also the surface chemical states are apparently modified. The comparison of peaks recorded after 6 min argon ion etching of the different silicides is illustrated in Fig. 2e). Clearly, the modified Ni $2p_{3/2}$ line position for ion etched $NiSi_2$, NiSi and Ni_2Si in the steady state can still be used as a fingerprint for correct phase identification. However, the Ni $2p_{3/2}$ peak shifts with respect to that of metallic Ni are different in these two cases, i.e. with and without argon ion etching.

2.2 Thermodynamics of Ni-Si-C system

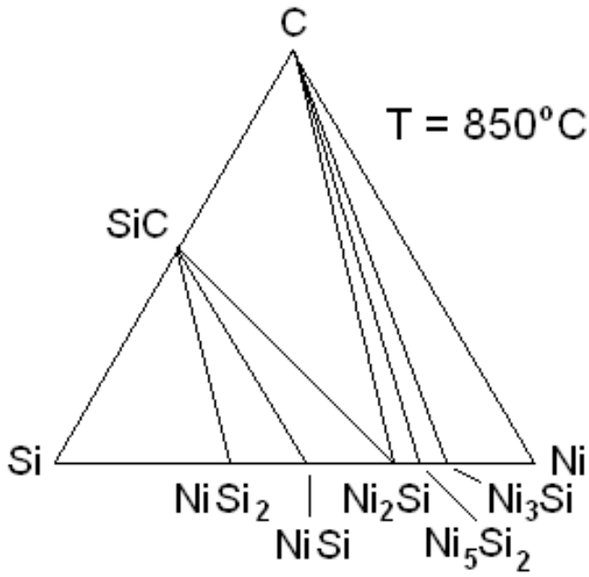

Fig. 3. Isothermal section of the Ni-Si-C at 850°C (La Via et al.; 2002).

Figure 3 shows the equilibrium isothermal section of the ternary Ni-Si-C phase diagram at 850°C, which is characterised by the absence of both Ni-C compounds and ternary phase. Furthermore, only Ni_2Si can be in equilibrium with both C and SiC.

The elements Si and Ni have a strong affinity to one another. The thermodynamic driving force for the Ni/SiC reactions originates from the negative Gibb's free energy of nickel silicide formation. However, the strong Si-C bond provides an activation barrier for silicide formation. It is necessary to break the Si-C bonds before the reaction. Moreover, the interfacial energy of C/Ni-silicide is also positive and need to be overcome. Silicide formation can therefore only be expected at higher temperatures when enough thermal energy is available, and the activation barrier can be overcome completely.

The expressions for the Gibb's energies ΔG (Lim et al., 1997) for the various reactions within the Ni-Si-C system are illustrated in Table 1. Considering the reaction between SiC and Ni from room temperature to ~ 1600K, the formation of Ni_2Si shows the most negative ΔG value, and can thus occur by solid state reaction relatively more easily. Free C is liberated at the same time.

Possible reactions	Gibb's energy as a function of temperature T (kJ/mol Ni)
$Ni+\frac{1}{3}\ SiC \rightarrow \frac{1}{3}\ Ni_3C+\frac{1}{3}\ Si$	30.793 + 0.0018 ·T ·logT - 0.0103 ·T
$Ni+2SiC \rightarrow NiSi_2+2C$	22.990 + 0.0108 ·T ·logT - 0.0454 ·T
$Ni+SiC \rightarrow NiSi+C$	-30.932 + 0.0054 ·T ·logT - 0.0195 ·T
$Ni+\frac{2}{3}\ SiC \rightarrow \frac{1}{3}\ Ni_3Si+\frac{2}{3}\ C$	-38.317 + 0.0036 ·T ·logT - 0.0158 ·T
$Ni+\frac{1}{2}\ SiC \rightarrow \frac{1}{2}\ Ni_2Si+\frac{1}{2}\ C$	-41.8 + 0.0027 ·T ·logT - 0.0119 ·T

Table 1. Possible reactions and their Gibb's free energies (ΔG_T) for the reaction between SiC and Ni. (Lim et al., 1997)

2.3. Bulk Ni-SiC diffusion couple

The interface reactions between bulk SiC and bulk Ni metal diffusion couples have been studied by several authors (see e.g. refs. Backhaus-Ricoult, 1992; Bhanumurthy & Schmid-Fetzer, 2001; Park, 1999). In the reaction zone, it has been observed that the diffusion couple shows alternating layers of C and Ni-silicides (900°C, 24 h or 40 h) (Bhanumurthy & Schmid-Fetzer, 2001; Park et al., 1999), or alternating silicide bands and silicide bands with embedded C (950°C, 1.5 h) (Backhaus-Ricoult, 1992). From the back-scattered electron imaging (BSE) (Park et al., 1999) of a Ni/SiC reaction couple annealed at 900°C for 40 h, the sequence of phases in bulk diffusion couples was observed to be $Ni/Ni_3Si/Ni_5Si_2+C/Ni_2Si+C/SiC$. The approximate width of the bands was about 5-10 μm. A schematic BSE image of SiC/Ni reaction couple annealed at 900°C is shown in Fig. 4. $NiSi_2$ is not observed because of the positive Gibb's free energies for its formation at the temperature studied, see Table 1. The absence of NiSi phase, however, is probably due to the insufficient annealing

(kinetic reason) used by the author since the thermodynamic conditions are met. NiSi has been observed in the thin film Ni-SiC system.

The formation of Ni_2Si follows the parabolic rate law $d = kt^{1/2}$ (d: thickness of silicide, k: parabolic rate constant, t: time) with $k = 6.27 \times 10^{-8}$ cm^2/s at 950°C (Backhaus-Ricoult, 1992). This means that the global reaction is diffusion-controlled. Nickel is the mobile species in Ni_2Si and its diffusion via its own sub-lattice by the vacancy mechanism is supposed to control the Ni_2Si growth (Ciccariello et al., 1990). The activation energies for Ni lattice and grain boundary diffusion have been found to be 2.48 eV and 1.71 eV, respectively. The diffusion of Ni along grain boundary is thus more important in the formation of Ni_2Si. The formation of NiSi is also diffusion controlled, while that of $NiSi_2$ is nucleation controlled (Lee et al., 2000).

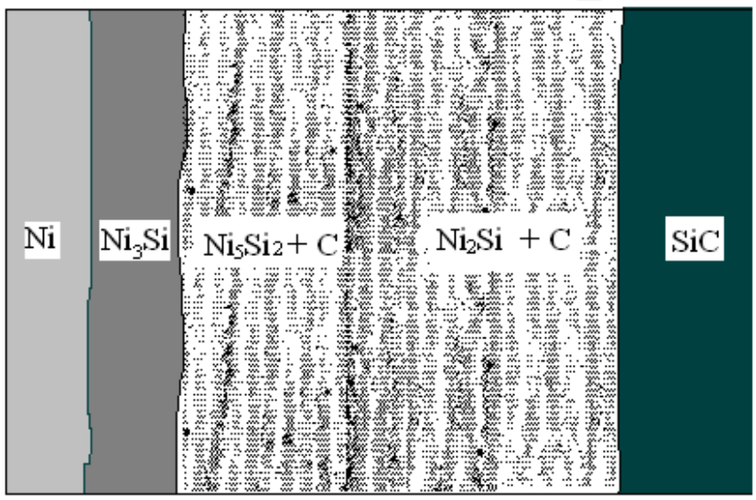

Fig. 4. Schematic BSE image of SiC/Ni reaction couple annealed at 900°C for 40 h (Park et al., 1999)

The formation mechanism of periodic bands is not very clear, but it is generally accepted that it depends on the diffusivities of the reacting elements. Metal is the most dominant diffusing species and C atoms are practically immobile (Bhanumurthy & Schmid-Fetzer, 2001; Park et al., 1999). After the formation of silicide, the Ni concentration at the SiC reaction interface decreases [Chou et al., 1990]. In order to further decompose SiC, the critical concentration level of Ni has to be satisfied. At the same time, the C, in front of the SiC reaction interface, forms small clusters and aggregates as a layer to minimize the interfacial energy. The continuation of this process will give rise to the formation of alternating Ni-silicide and C layers. The systems which show the tendency of the formation of periodic bands have relatively large parabolic rate constant k and k_0 values (intercept of the linear ln k versus 1/T plot) (Bhanumurthy & Schmid-Fetzer, 2001).

2.4. Ni film on SiC

2.4.1. Reaction products

A number of studies of the interfacial reactions between a Ni film and SiC have been reported (see e.g. Ohi et al., 2002; Gasser et al., 1997; Roccaforte et al., 2001; Madsen et al.,

1998; Litvinov et al., 2002; Marinova et al., 1996 & Cao et al., 2006). The dominant phase formed is almost independent of the polytype, the polarity of the SiC and the details of the annealing cycle.

In the Ni/SiC system, Ni reacts with SiC to form Ni silicides and C. Dissociation of SiC occurs at around 500°C (Kurimoto & Harima, 2002). Generally, Ni_2Si is the dominant species in a large temperature range between 600 and 950°C (Ohi et al., 2002; Gasser et al., 1997; La Via et al. 2002; Abe et al., 2002; Roccaforte et al., 2001; Cao et al., 2006 & Kestle et al., 2000), as shown in the X-ray diffraction (XRD) spectra in Fig. 5. Similar as thin film Ni-Si system, silicides is formed sequentially, i.e. one compound is formed first and the second starts to form later on during the annealing. The phase sequence is $Ni_{23}Si_2$+$Ni_{31}Si_{12}$ → $Ni_{31}Si_{12}$ → $Ni_{31}Si_{12}$+Ni_2Si → Ni_2Si (Madsen et al., 1998 & Bächli et al., 1998). This is the reason why $Ni_{31}Si_{12}$ has been found at the surface in some cases, see eg. Refs. (Han & Lee, 2002; Han et al., 2002). Silicon rich silicides can be observed at the interface of Ni_2Si and SiC (Cao et al., 2005). Increasing temperature to above 1000°C results in the formation of a NiSi thin film (Litvinov et al., 2002; Kestle et al., 2000 & Marinova et al., 1996).

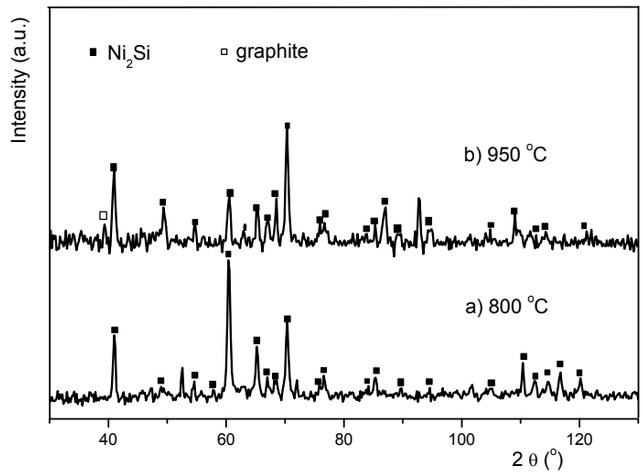

Fig. 5. XRD spectra of samples with ~ 100 nm Ni thickness on 4H-SiC after annealing. Glancing angle 3° with Cr k_α radiation (λ = 2.29Å)

2.4.2. Formation of Ni_2Si and its mechanisms

In the Ni/SiC system, the formation of Ni_2Si through the reaction 2Ni+SiC = Ni_2Si+C may consist of two stages (Cao et al., 2006) which are controlled by reaction and diffusion rate respectively.

The thermodynamic driving force for the Ni/SiC reaction originates from the negative Gibb's energy of Ni-silicide formation (Table 1). Before the formation of Ni_2Si by solid state reaction, however, it is necessary to break SiC bonds. The existence of Ni may help the dissociation of SiC at the temperatures lower than its dissociation value. It is known that the thermal expansion coefficient of SiC is 3-4 times higher than that of Ni (Adachi, 2004). This expansion difference results in thermal strain at higher temperatures for SiC sample coated with Ni, which corresponds to compression at the Ni side and tensile at the SiC side. It is thus possible that some Ni atoms slightly penetrate into the SiC side at the interface with the

help of the thermal energy. The theoretical calculation on the chemical bonding in cubic SiC (Yuryeva & Ivanovskii, 2002) has shown that Ni impurities weaken the covalent character of the SiC crystal, resulting in a decrease in the stability of the SiC adjacent to the Ni layer. The decomposition of SiC, which starts at the interface, is therefore possible at a temperature lower than its dissociation value. However, the stability of SiC must be lowered to certain degree before the decomposition of SiC. In other words, an incubation period exists. Following the decomposition of the SiC, Si and C released will diffuse into the Ni due to the expected low diffusion coefficient of the Ni in SiC. This has been proved by the expansion of metal Ni lattice prior to the appearance of Ni silicides in ultra thin Ni/SiC system (Su et al., 2002; Iwaya et al., 2006). The opposite Ni flux into the SiC may not be dominant in this stage. The mixture of Si and Ni occurs very rapidly, provided Si atoms are available. In fact, an amorphous interlayer (~ 3.5 nm) which is a mixture of Ni and Si has been observed in the Ni/Si system even at room temperature by solid-state diffusion (Sarkar, 2000). Therefore, the formation of new phase Ni_2Si in the first stage is determined by the speed of bond breakage, i.e., by the supply of Si from the decomposition of SiC. This is a reaction-rate controlled process.

With the progress of the reaction, heat is released by the formation of Ni_2Si. More SiC is then decomposed and more Si atoms become available. The supply of Si atoms is then no longer the dominant factor in the formation of Ni_2Si, because Ni is the dominant diffusing species through Ni_2Si (Ciccariello et al., 1990). The growth of thin Ni_2Si films is controlled mainly by the diffusion of Ni along the silicide grain boundaries. Nickel is then provided at the Ni_2Si/SiC interface where the silicide formation takes place. This interface advances by the arrival of new Ni atoms. The formation obeys the parabolic rate law. In this case, the Ni flux increases relative to fluxes of Si and C from SiC and the mechanism of reaction changes to a diffusion controlled one, corresponding to the second stage of the reaction.

In addition, the Ni_2Si formed by annealing possesses textured structure to some degree, which was confirmed by XRD [Cao et al., 2006].

2.4.3. Formation of C and its chemical states

After the reaction between Ni and SiC, C present in the consumed SiC layer should precipitate. A number of studies of the chemical state of C after annealing have been reported (Gasser et al., 1997; La Via et al, 2003; Han & Lee, 2002; Marinova et al, 1996; Marinova et al, 1997). Figure 6a) shows the C1s XPS region spectra at the surface after heat treatment at 800°C and 950°C in vacuum. It is seen that C is mainly in the chemical state analogous to that of graphite in the surface region for both temperatures (Cao et al. 2006). To investigate further the chemical states of the C species inside the contact, C1s XPS peaks have been recorded after successive Ar ion etchings, as shown in Fig. 6b. It is revealed that the C1s binding energy value recorded from the sample heated at 950°C was slightly higher than that from lower temperature, implying the possible difference of the chemical state. Considering binding energy of C1s XPS peak decreases with decreasing structure order in C species (Rodriguez et al, 2001), a less ordered structure below the surface could be possible in the case of 800°C heat treatment. Further evidence can be obtained by means of Raman spectroscopy, as shown in Fig. 7. Compared with graphite standard, the broadened and shifted G and 2D peaks as well as the appearance of an additional D peak indicate the

formation of nanocrystalline graphite cluster in annealed Ni-SiC samples (Cao et al, 2006). This is consistent with the result of Kurimoto and Harima (Kurimoto & Harima, 2002). Close examination of line position and shape of G and 2D Raman peaks together with the intensity ratio I_D/I_G obtained at different temperatures indicate that more highly graphitised and less disordered carbon is promoted by a higher annealing temperature at 950°C. Similar results have been reported in ref. (Ohi et al, 2002; Kurimoto & Harikawa, 2002). For temperatures of 600 and 800°C, Ohi et al. found the formation of C with modified π bonds when compared to graphite. The π sub-band has different density of states from that of graphite.

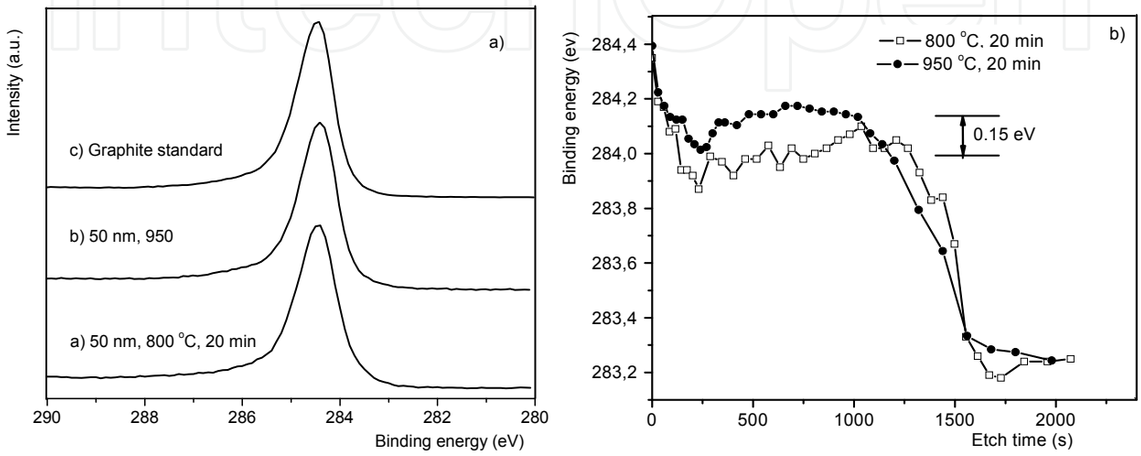

Fig. 6. a). C1s XPS spectra at the surface; b) C1s XPS peak position recorded by successive Ar ion etchings. Ni/4H-SiC samples annealed in vacuum. t_{Ni} = 50 nm. The etch rate calibrated on Ta_2O_5 under the experimental condition is 5.6 nm /min.

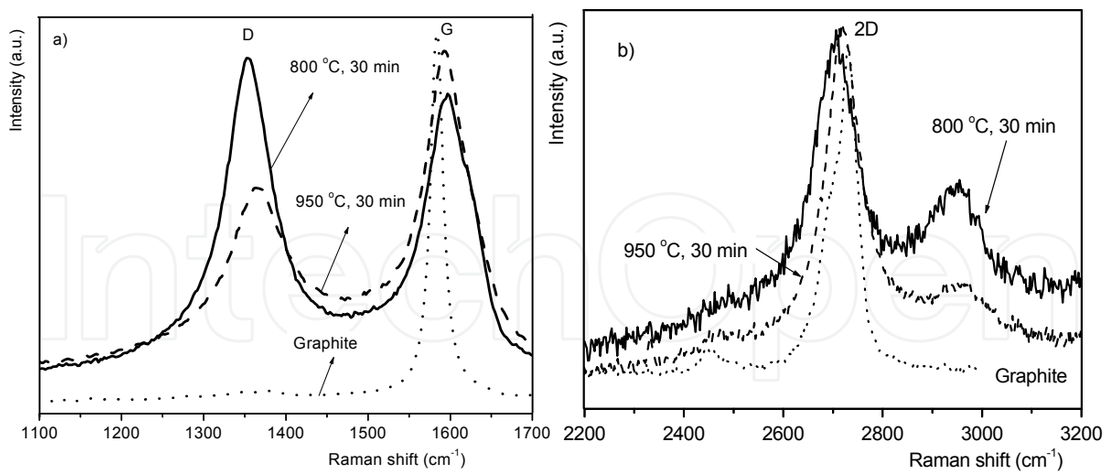

Fig. 7. Raman first-order a) and second-order b) spectra of graphite and vacuum annealed Ni-4H SiC samples. t_{Ni}= 200 nm.

In the process of formation of C, Ni acts as an effective catalyst for graphitisation (Lu et al, 2003). In fact, once silicide has formed, not only can Ni act as mediating agent but also the reaction product, the silicides (Hähne & Woltersdorf, 2004), can do so. The driving force for

the graphitisation process is the decrease of free energy by the conversion of amorphous C to graphite. The graphitisation process is a gradual disorder-order transformation. It includes the rearrangement of disordered C atoms, released from the formation of silicide, to hexagonal planar structures and the formation of ordered stacking structures along c axis. The structure of C is less complete at lower temperature.

2.4.4. Distribution of phases in the reaction products and the effect of pre-treatment and Ni layer thickness

Carbon is released from the SiC during the silicide formation. The redistribution of C after annealing is one of the most controversial aspects in studying the Ni/SiC reactions. The main opinions are: a) Carbon atoms are distributed through the contact layer and accumulated at the top surface (Kurimoto & Harima, 2002; Han & Lee, 2002; Bächli et al., 1998; Han et al., 2002). b) Carbon in graphite state is present in the whole contact layer with a maximum concentration at the contact/SiC interface (Marinova et al., 1997). c). Carbon agglomerates into a thin layer far from the silicide/SiC interface after annealing (La Via et al., 2003). d). Carbon is almost uniformly distributed inside the silicide layer (Roccaforte et al., 2001).

To authors' opinion, the C distribution is dependent on several factors, such as annealing environment, pre-treatment on SiC substrate and Ni layer thickness. The in-situ depth profiles by XPS study for vacuum annealed Ni/SiC sample without exposure to the air reveal that there is a C layer at the external surface in all cases, as shown in Fig. 8 and 9 (Cao et al., 2005; Cao et al, 2006, Cao & Nyborg, 2006). The carbon diffuses mainly through the non-reacted Ni film towards the external surface at the beginning of reaction. The external surface acted as an effective sink for C accumulation. According to the Ellingham diagram, the equilibrium partial pressure of oxygen for reaction $2C + O_2 = 2CO$ at 800°C is ~ 10^{-20} atm (Shifler, 2003), which is much lower than the partial pressure of oxygen in the normal vacuum annealing furnace (~10^{-9}-10^{-10}atm). The driving force for the C moving to the free surface is thus provided. In the equilibrium state, the C at the free surface will disappear by reacting with oxygen to form CO. However, some C still exists and is thus in a metastable state. Besides the experimental error, one possible reason for the discrepancies in the literature regarding C distribution could be the annealing atmosphere having different reactivity with C. The use of unsuitable analysis methods, such as EDX, could also be a cause.

The surface pre-treatment of the SiC substrate has certain influence on the C distribution (Cao et al., 2005; Cao et al., 2006). In the case of SiC substrate without pre-treatment or with chemical cleaning, the in-situ depth profile obtained is illustrated in Fig. 8. For very thin Ni layers (less than ~ 10 nm), a C-depleted zone separates a thin C surface layer from the SiC substrate (Fig. 8a). For thicker Ni layers, a further accumulation of C is also observed below the surface region (Fig. 8b). The maximum C concentration is away from the silicide/SiC interface at a certain distance. The reason is as follows. After a continuous layer of silicide with certain thickness has formed, the rate of accumulation of C to the free surface decreases due to the expected low diffusivity of C in silicide. It is known that the diffusion coefficient of C in Ni at 800°C is 1.6×10^{-8} cm^2s^{-1} (Smithells, 1967). However, the diffusivity of C in N–doped n–type hexagonal SiC at 800°C extrapolated from the data at 1850-2180°C is as low

as 1.1×10^{-31} cm^2s^{-1} (Matzke & Rondinella, 1999). Carbon is therefore much more mobile in metal Ni than in 4H–SiC. As the Ni_2Si/SiC interface advances, C phase is also buried within the silicide. To minimize the total interfacial energy between C and Ni-silicide, the C phase would tend to form clusters in the direction opposite to the external surface as well (Fig. 8b).

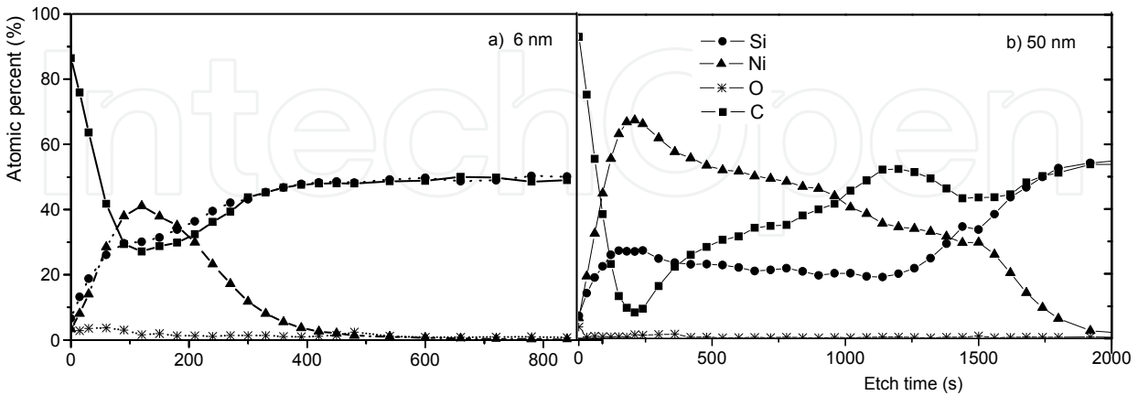

Fig. 8. In-situ depth profiles of samples with Ni layer thickness a) 6 nm and b) 50 nm (Cao et al., 2006). The samples were heated at 800°C for 20 min in vacuum. The SiC substrate is in the as-delivered state from manufacturer. The etch rate calibrated on Ta_2O_5 under the experimental condition is 5.6 nm /min.

However, for the sample experiencing Ar ion etching before the Ni deposition there is a different phase distribution in the reaction product (Fig. 9). The argon ion bombardment deposited a large amount of energy on the surface and created many excitations, including ionization of secondary ions and neutral particles and ejection of electrons. All these energetic particles could in principle transfer energy into SiC and facilitate its dissociation. The energetic particles mentioned above might also provide energy to enhance the diffusion of the Ni atoms into the bulk. It is known that nickel is the dominant diffusion species in nickel silicides and controls the rate of Ni_2Si formation in the second reaction stage. As a result of fast dissociation of SiC and enhanced diffusion of Ni, Ni_2Si is formed quicker under the action of argon ion pre-treatment. Consequently, there is less C agglomerated at the surface because C is much less mobile in Ni_2Si than in metal Ni.

For the thinnest Ni layer (d_{Ni} = 3 nm), heat treatment lead to the formation of surface graphitic carbon layer and silicide below with low carbon content (Fig. 9a). With the Ni thickness doubled to 6 nm (Fig.9b), there is a carbon rich layer below the surface region, which is clearly different from Fig. 8a. In Fig. 9c (d_{Ni} = 17 nm), a silicide layer with carbon deficiency develops adjacent to the interface. The maximum C content is ~ 4 nm away from the silicide/SiC interface. Increasing Ni thickness even more results in a repeated maximum of carbon intensity corresponding to the minimum of the nickel intensity, i.e., a multi-layer structure, consisting of silicide rich layer/ carbon rich layer / silicide rich layer / ⋯⋯ (Fig. 9d). The silicide layer adjacent to the interface is deficient of C. The depth profiles indicate that there is a minimum Ni thickness (~ 15 nm) for the formation of such multi-layer structure. The development of such a structure can be explained by the quicker formation of Ni_2Si under such a condition. It is then difficult for free C released from the SiC to move long distance due to the low diffusivity and low solid solubility of C in silicide. In order to

minimize the interfacial energy between C and Ni-silicide, as a compromise, the dissociated C atoms might form small clusters and aggregated as a layer.

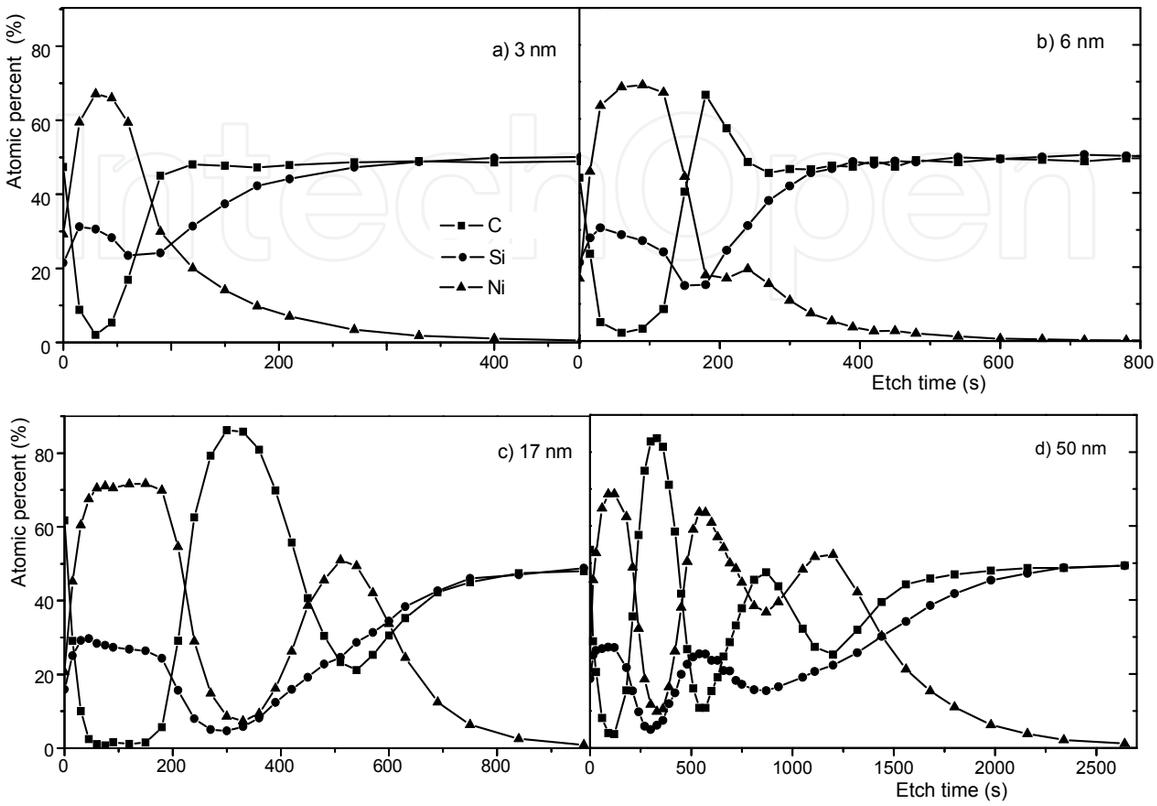

Fig. 9. In-situ depth profiles of samples with different Ni layer thickness (Cao et al., 2005). The SiC substrate was cleaned by Ar ion etching with 4 keV energy before Ni deposition. The samples were then heated at 800°C for 20 min in vacuum. The etching rate calibrated on Ta_2O_5 under the experimental condition is 5.6 nm /min.

It is also interesting to identify the silicide (Ni_2Si) morphology for thin Ni film samples. Figure 10 presents the Si2p peak from Ni/SiC samples with different Ni layer thickness (Cao et al., 2006). After annealing thin Ni layer sample (t_{Ni} = 3 nm) at 800°C for 20 min in vacuum, it is known from XPS curve fitting results that the Si2p peaks are composed of three chemical states (Fig. 10 a): the main part being Si in SiC, and the other two small parts being Si in SiO_2 and Ni_2Si, respectively. The existence of SiO_2 is due to the slight oxidation in the furnace. Considering that the deposited Ni film is continuous and uniform, the appearance of strong carbide signal (from Si in SiC) suggests that Ni_2Si tended to form islands during the annealing. With the Ni thickness doubled (Fig. 10b), the amount of Ni_2Si increases obviously and the detected amount of SiC decreases. The Ni silicide island can grow both laterally and vertically. Increasing Ni thickness even more (Fig. 10c) results in the disappearance of SiC signal and Ni_2Si is dominant. The above results indicate that the silicide becomes continuous with increasing Ni film thickness.

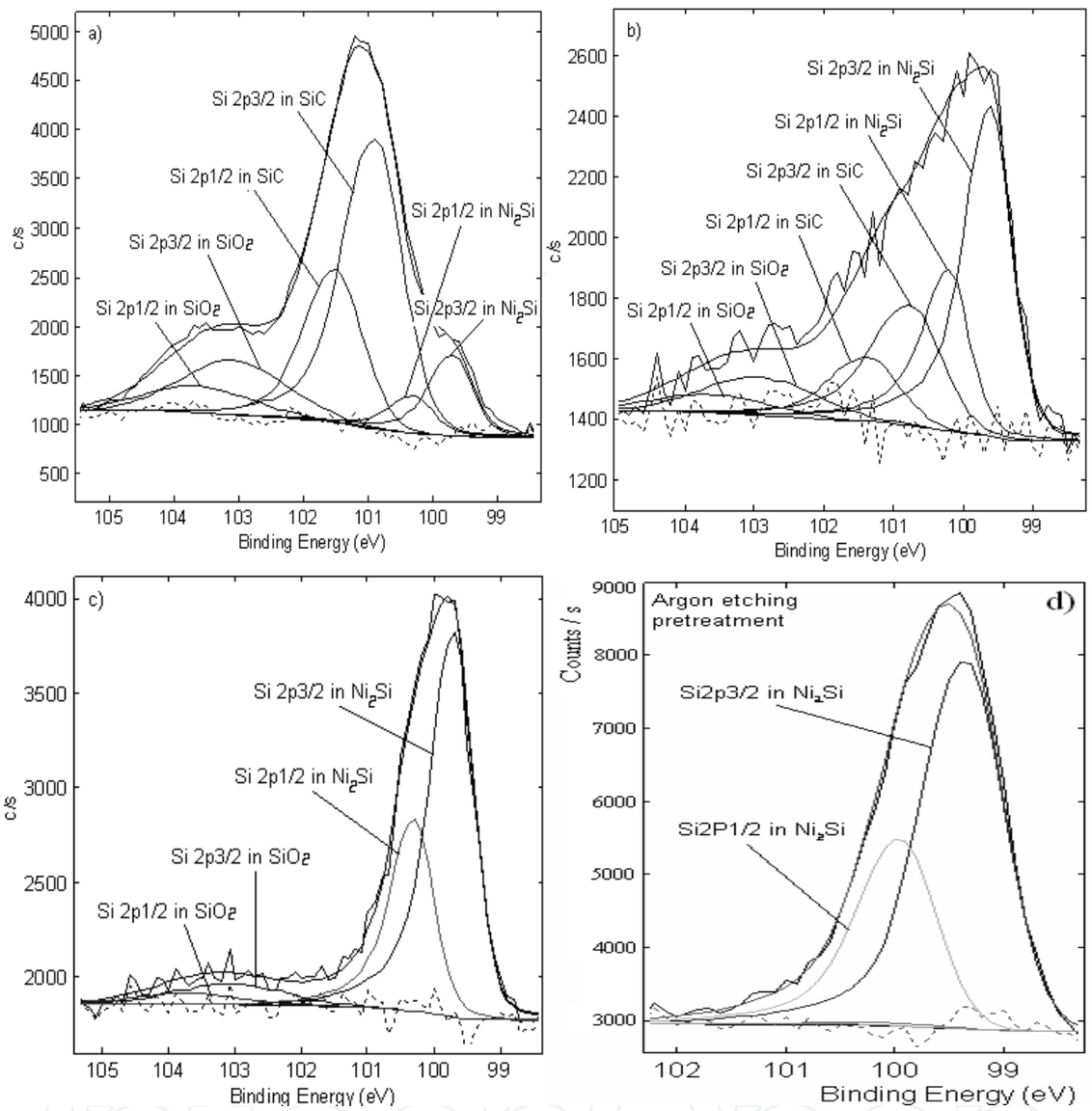

Fig. 10. In-situ Si2p XPS spectra of Ni/SiC samples after annealing at 800°C for 20 min in vacuum. a) t_{Ni} = 3 nm b) t_{Ni} = 6 nm c) t_{Ni} = 17 nm d) t_{Ni} = 6 nm. In Fig. a-c), the Ni thin films were deposited on as-delivered SiC substrate. In Fig. d), the SiC substrate was cleaned by Ar ion etching with 4 keV energy before Ni deposition.

Fig. 10b) and d) give the XPS Si 2p peak recorded from the samples with same initial Ni layer thickness (d_{Ni} = ~ 6 nm) but different pre-treatment on SiC substrate. From the comparison it has been found that the shoulder at higher binding energy representing Si in SiC disappears when the Ni thin film is deposited on an argon ion etched SiC substrate. This is again related to the fast dissociation of SiC and enhanced diffusion of Ni under the action of argon ion pre-treatment. The nucleation and growth of Ni_2Si are promoted. Therefore, the silicides formation kinetics is affected and a continuous silicide layer develops quicker.

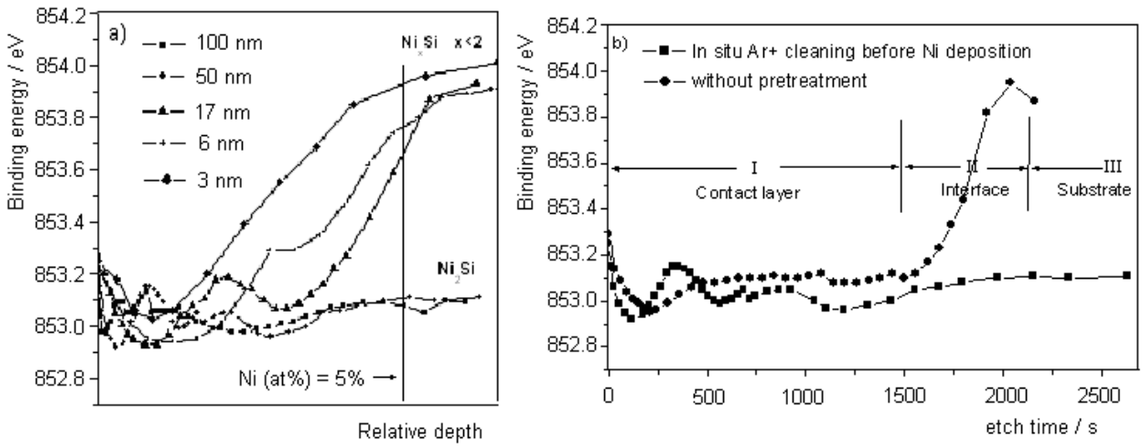

Fig. 11. Binding energy of Ni $2p_{3/2}$ peaks as function of (a) Ni layer thickness (the SiC substrate was cleaned by Ar ion etching with 4 kev energy before Ni deposition), and (b) pre-treatment (d_{Ni} = 50 nm)

The silicides formed at the interface depend also on the Ni layer thickness and the pre-treatment on SiC substrate prior to the Ni deposition. Figure 11 shows the development of Ni $2p_{3/2}$ peak position as function of initial Ni layer thickness and pre-treatment. From Fig.11 a), we see that for thin Ni layers (d_{Ni}= 3, 6, 17 nm), NiSi, $NiSi_2$ or even higher Si containing silicides are formed at the interface. It has been known that higher amount of Si in the silicides gives higher binding energy position (Fig. 2e). The reason why Si-richer silicides are formed may be attributed to the considerable consumption of nickel. Because the metal supply is likely to be more limited, one could expect the formation of Si-richer silicides following Ni_2Si. Anyway, the total amount of Si rich silicide is small because of the low availability of Ni near the interface. For fixed Ni film thickness (50 nm), the influence of argon ion etching pre-treatment on the type of interfacial silicide is shown in Figure 11b). In the contact layer (I), the binding energy fluctuation (as also observed in Fig. 11 a) results from the effect of ion bombardment (at the beginning) and the alternating composition changes in depth (see Fig. 9). At the interface (II), the sample without pre-treatment has higher Ni $2p_{3/2}$ binding energy value. This implies that a compositional gradient existed and that Si-richer silicides are formed at the interface. The reason may be also attributed to the limited availability of nickel. On the other hand, argon ion etching pre-treatment enhances the Ni diffusion and accelerate the supply of Ni and almost keeps the same kind of silicide all the time.

3. Ta (or Ni/Ta)-SiC

Tantalum (Ta) is a refractory metal with high melting point (around 3000°C) and it exhibits two crystalline phases, bcc α-phase and tetragonal β-phase. The α-phase has high toughness and ductility as well as low electrical resistivity and corrosion resistance, while the β-phase is hard and brittle and less desirable. Tantalum can form both stable carbides and silicides with attractive properties with respect to oxidation resistance and general physical behaviour. There exist two stable carbides in the Ta-C system, Ta_2C and TaC, with the

melting points of 3330°C and 3985°C, respectively. Both these carbides are interstitial compounds and thermally very stable. For example, TaC has been used for reinforcing Ni superalloys (Berthod et al., 2004). The research on contacts involving Ta on SiC is not as extensive as that on Ni contacts. Attempts have been made to create ohmic contacts on SiC by using elemental Ta, and its silicide or carbide (Olowolafe et al, 2005;, Guziewicz, 2006, Jang et al., 1999; Cao et al, 2007[a,b]).

3.1 Thermodynamics of Ta-Si-C system

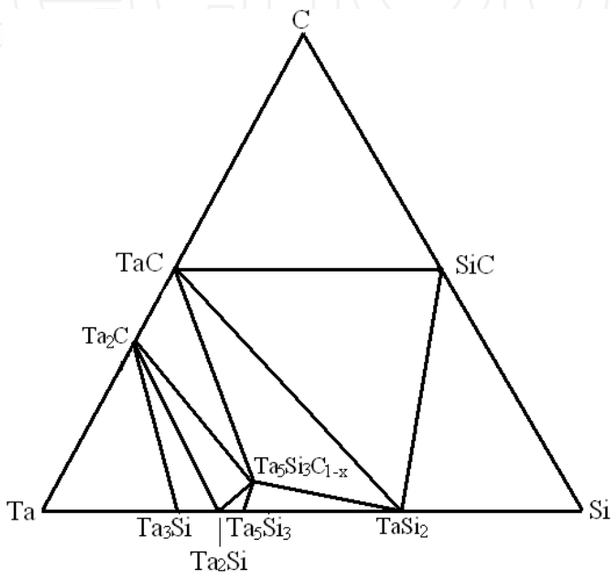

Fig. 12. Simplified isotherm ternary phase diagram of Ta-Si-C at 1000°C (Schuster, 1993-1994).

An isothermal section of Ta-Si-C at 1000°C is shown in Fig. 12 (Schuster, 1993-1994). It might apply at temperatures up to 1827°C (Brewer and Krikorian, 1956). It can be seen from the figure that SiC can be in equilibrium with both TaC and $TaSi_2$. The author proposed the existence of a ternary compound $Ta_5Si_3C_{1-x}$ ($x \approx 0.5$) which can coexist with TaC, Ta_2C, Ta_2Si, Ta_5Si_3 and $TaSi_2$. However, the status of this compound is in doubt (Laurila et al., 2002), since it is not clear if it is a real ternary compound or simply the metastable Ta_5Si_3 with carbon solubility.

Compound	ΔH (kcal/g atom)*	Reaction	ΔH_R (kcal/g atom)*
SiC	-26.7	$4Ta+SiC = Ta_2C+Ta_2Si$	- 4.9
Ta_2Si	-10.1	$3Ta+SiC = TaC+Ta_2Si$	-4.3
Ta_5Si3	-9.0	$5Ta+2SiC = 2Ta_2C+TaSi_2$	-5.2
$TaSi_2$	-8.0	$3Ta+2SiC = 2TaC+TaSi_2$	-4.4
Ta_2C	-46	$11Ta+3SiC = 3Ta_2C+Ta_5Si_3$	-3.9
TaC	-38		

*ΔH: Standard heats of formation
ΔH_R: Enthalpy change for the reaction of Ta and SiC at 800°C.
Table 2. Thermodynamic data in Ta-Si-Ta system (Geib et al., 1990)

The thermodynamic driving force for the Ta/SiC reactions also originates from the negative Gibb's free energy of Ta silicide or carbide formation. The standard heats of formation and calculated enthalpy changes, ΔH_R, for the various reactions within the Ta-Si-C system are illustrated in Table 2 (Geib et al., 1990). It can be seen that the standard heats of formation of Ta carbides Ta_2C and TaC are larger than that of SiC. Assuming the entropy contribution to be small, the change of Gibb's free energy can be approximated by ΔH_R. The negative values at this temperature imply that the reaction between Ta and SiC is energetically favorable.

3.2 Reaction between Ta film and SiC

Table 3 summarizes the evolution of the thermal reaction between Ta film and SiC substrate up to 1200°C (Chen et al., 1994, Cao et al., 2007[a]). Similar phase sequence has been reported (Feng et al., 1997) for SiC/Ta/SiC couples at 1500°C, while α-Ta_5Si_3 was not observed. Ta_5Si_3:C here is a carbon-stabilized phase with a hexagonal Mn_5Si_3 structure according to the XRD powder diffraction database. It is in fact the same compound as the ternary compound $Ta_5Si_3C_x$ reported by some researchers.

Temperature / time	Reaction products in Ta/SiC system	Reaction products in Ni/Ta/SiC system	Initial film thickness on SiC
650 °C /0.5 h	Ta	Amorphous Ni-Ta, Ta, Ta_2C	100 nm
800 °C /0.5 h	Ta + Ta_2C	Ta_2C, Ta_5Si_3:C, Ta(?)	100 nm
900 °C / 1 h	Ta + Ta_2C + Ta_5Si_3:C		320 nm
950°C/0.5 h	Ta + Ta_2C + Ta_5Si_3:C	Ta_2C, TaC, Ta_5Si_3:C, Ta_5Si_3, TaNiSi, Ni_2Si	100 nm
1000 °C/1 h	TaC + Ta_5Si_3:C + α-Ta_5Si_3 + Ta_2C		320 nm
1100 °C/0.5 h	TaC + Ta_5Si_3:C		320 nm
1200 °C/1 h	TaC + $TaSi_2$		320 nm

Table 3. Evolution of the thermal reaction between Ta (or Ni/Ta) and SiC (Chen et al., 1994, Cao et al., 2007[a,b]). In Ni/Ta/SiC system, the thickness ratio of Ni:Ta is ~3:5.

One important feature in the thin film Ta/SiC system is the development of layered structure at high temperatures. Figure 13 shows the Auger depth profiles obtained after annealing at different temperatures in vacuum. Compared to the as-deposited film (Fig. 13a), less sharp interface in Fig. 13b suggests that inter-diffusion has occurred at 650°C. Carbon, which corresponds to the formation of Ta_2C carbide, is observed in the contact layer after annealing at 800°C (see Fig. 13c). Clearly, more Ta_2C is formed at 950°C (Fig. 13d). No Si signal is detected in the near surface region, confirming the lack of silicide on the top surface. This can be further confirmed by the XRD analyses at 950°C (Fig.14), in which Ta_5Si_3:C is not able be observed by using grazing angle 1°. However, it can be detected by using grazing angle 3°. Ta_5Si_3:C must tend to form at a certain distance below the surface. A mixture layer of Ta_5Si_3:C and Ta_2C is present there. The reaction zone is shown to have a layered structure of $Ta_2C/Ta_2C+Ta_5Si_3$:C/SiC after heating at 950°C (Cao et al., 2007[a]). With the temperature increasing to 1000°C, it changes to a well defined four-layered structure Ta_2C/α-Ta_5Si_3/Ta_5Si_3:C/TaC/SiC (Chen et al., 1994). In fact, the layered structure is inclined to form when the vanadium group metals (V, Nb and Ta) react thermally with SiC at high

temperatures. The layered structure can be attributed to the requirement of the minimization of the interfacial energy.

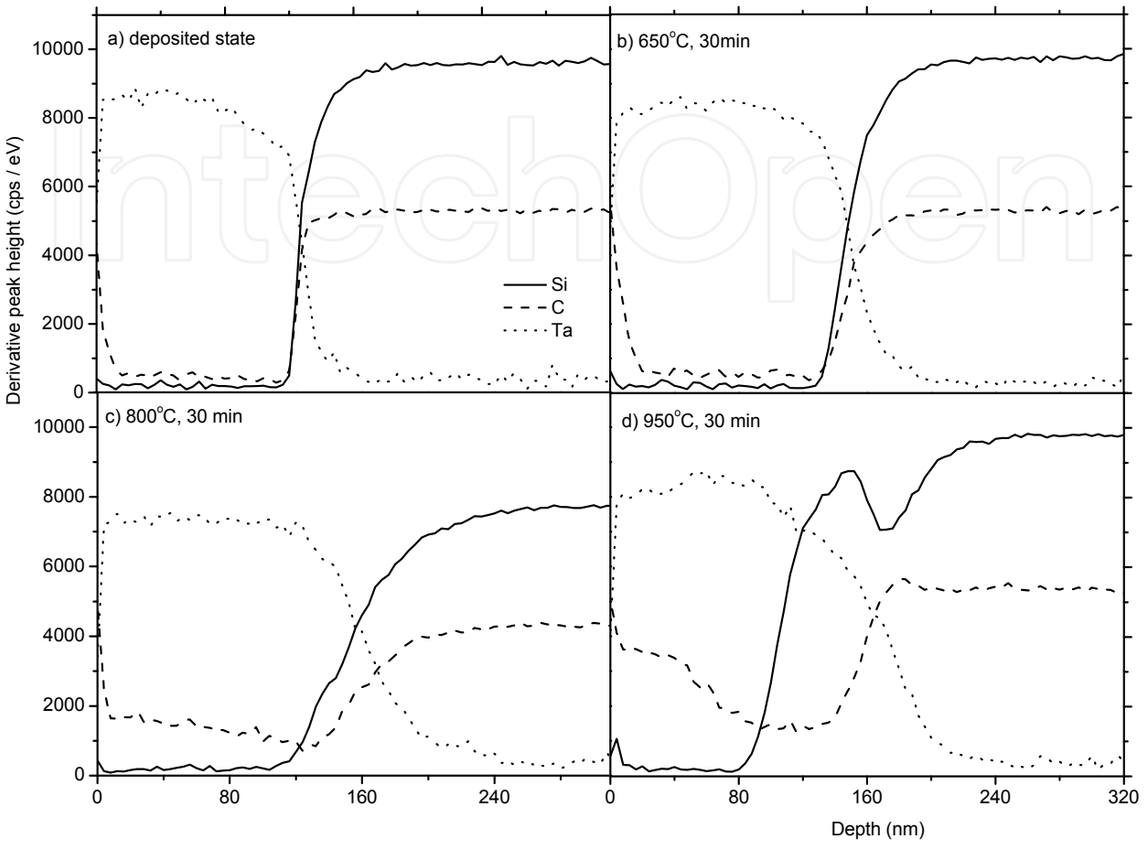

Fig. 13. Depth profiles of Ta/SiC before and after annealing in vacuum at different temperatures with Ta thickness of 100 nm. The depth scale is given by using the etch rate of Ta_2O_5 with known thickness under the same condition (8 nm/min).

Another important feature in the thin film Ta/SiC system is the formation of the C deficiency region in the near interface side of the SiC. The apparent atomic concentrations of C and Si in the thermal reaction product are given in Fig. 15 by considering the area percentages for the corresponding chemical states obtained from the curve fitting of XPS C1s and Si2p peak. The distribution of phases obtained at 800 and 950°C is further confirmed. Besides un-reacted metal Ta, as mentioned before, the reaction zone is shown to have a layered structure of $Ta_2C/Ta_2C+Ta_5Si_3$:C/SiC. Importantly, it can be seen that the total amount of C is higher than that of Si in the reaction layers formed at both 800 °C and 950°C. This means more C diffuses towards the Ta layer from the substrate. Carbon has a high diffusivity in Ta ($D = 6.7\times10^3 \exp(-161.6/RT)$ cm^2/s, for T = 463-2953K and R = 8.314 J mol^{-1} K^{-1}) (Le Claire, 1999). It is the dominant moving species and reacts more rapidly with Ta than Si. In other words, C deficiency region is preferentially produced in the near interface side of the SiC.

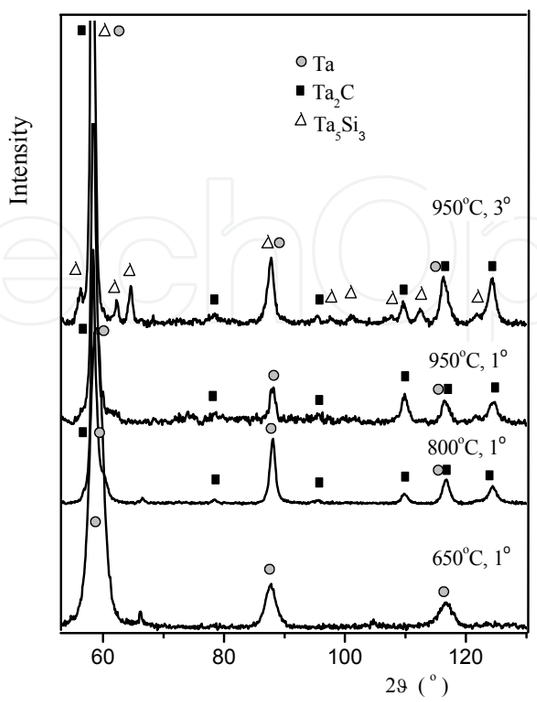

Fig. 14. Grazing angle XRD spectra with Cr k_α radiation of Ta/SiC after annealing in vacuum. The thickness ratio of Ni:Ta is ~3:5 and the total film thickness is ~100 nm.

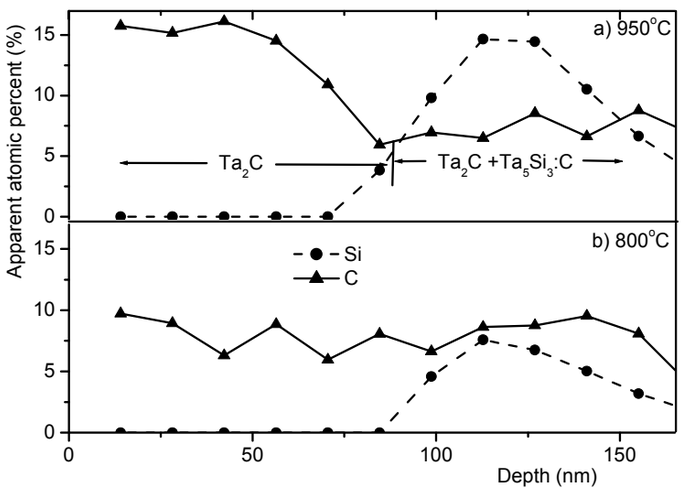

Fig. 15. Apparent atomic concentration of C and Si in the reaction layer with the depth. Ta/SiC samples with 100 nm Ta thickness were annealed at different temperatures in vacuum. Si and C from the SiC substrate are not included in the Fig. The depth is given by using the etch rate of Ta_2O_5. (Cao et al., 2007[a]).

3.3. Effect of Ni incorporation in thin film Ta/SiC system

Table 3 and Fig. 16 summarize the evolution of the thermal reaction between a dual metal Ni/Ta films on SiC substrate up to 950°C by means of grazing angle XRD. The deposited Ta and Ni films usually have crystalline structure. However, no reflection from metallic Ni can be observed for the samples treated at 650°. A broad diffraction peak in the region of 56-65° superimposed on the α-Ta and Ta_2C diffraction peaks (Fig. 16a) probably come from the amorphous phase produced by solid-state reaction. The driving force for amorphous phase formation is generally expected from the large negative enthalpy of mixing for the Ni/Ta system (Zhang et al., 2000). It has been reported that annealing polycrystalline Ni/Ta multilayers at between 673 and 773 K led to the formation of amorphous phase (Liu & Zhang, 1994; Hollanders et al., 1991). Amorphous Ni-Ta can also be achieved by mechanical milling (Lee et al., 1997), rapid quenching (Fedorov et al., 1986) and ion irradiation (Liu & Zhang, 1994). With increasing temperature, crystallization of Ni-Ta amorphous is expected. The crystallization temperature is related to the composition of the amorphous alloy and activation energy exhibits a maximum near the eutectic composition.

For the film annealed at 800°C (Fig. 16b) diffractions of Ta_2C and metastable carbon-stabilized Ta_5Si_3:C are observed. However, as certain Ta peaks overlap with those of Ta_2C, a minor amount of un-reacted Ta could also be present. It is difficult to ascertain any crystallised Ni-Ta compound or Ni silicide by the XRD pattern. Annealing at 950°C results in the presence of both the stable carbides Ta_2C and TaC (Fig. 16c), the latter of which is dominant. Ta_5Si_3:C and stable α-Ta_5Si_3 are also confirmed. In spite of the XRD peak overlapping, the formation of binary Ni_2Si and ternary TaNiSi silicides could be possible.

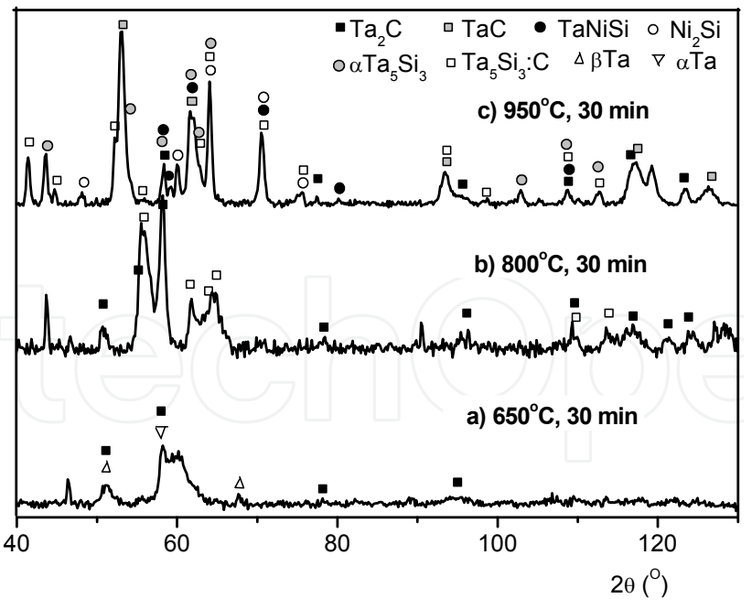

Fig. 16. Grazing angle XRD spectra of Ni/Ta films on SiC after annealing in vacuum. The thickness ratio of Ni:Ta is ~3:5 and the total film thickness is ~100 nm. Glancing angle 3° with Cr k_α radiation (λ = 2.29Å)

By comparison of the phases formed between Ta/SiC and Ni/Ta/SiC system at the same temperatures (Table 3), it is found that the dual layer Ni/Ta lowers the temperature at which Ta_2C, Ta_5Si_3:C, TaC or α-Ta_5Si_3 can be detected by grazing angle XRD. It is thus concluded that the existence of Ni promotes the reaction between Ta and SiC, lowering the formation temperature of Ta carbide and silicide.

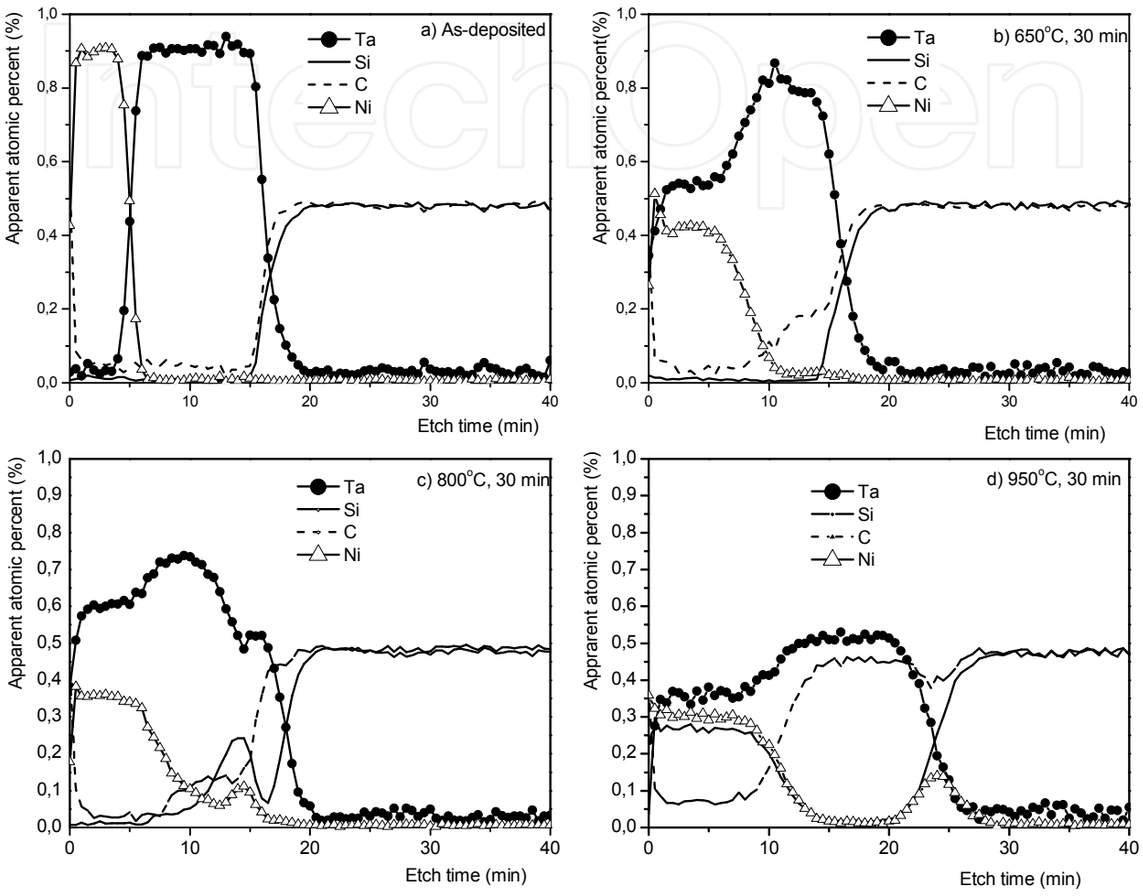

Fig. 17. Auger depth profiles of annealed Ni/Ta/SiC samples. The thickness ratio of Ni:Ta is ~3:5 and the total film thickness is ~100 nm. The etch rate calibrated on Ta_2O_5 with known thickness is 8 nm/min. The atomic concentration is obtained by using the measured Auger peak-to-peak intensities and relative sensitive factors deduced from the elementary intensities of the as-deposited sample.

Figure 17 gives the apparent atomic concentration vs. etch time. The as-deposited sample (Fig. 17a) possessed a rather sharp interface. Annealing at 650°C results in evident change of element distribution (Fig. 17b). The reaction zone is composed of two parts: an upper region of mainly Ni-Ta amorphous mixture and an inner region of metallic Ta and Ta_2C. The Ta_2C layer is supposed to be related to the fast diffusion of C being released from SiC. Apparently, as no Si is evident from the reaction layers within the depth profile, it is suggested that the C moves faster outwards through the coated layer and that it also reacts more readily with the deposited Ta. There is minor amount of Ni dissolved in the inner Ta

phase as well. The Ni can act as mediating agent to trigger readily the reaction between Ta and SiC. Compared to the Ta atom, the Ni atom has smaller size (atomic radii of Ni and Ta are 1.62Å and 2.09Å, respectively). Some dissolved Ni atoms might partially penetrate into the SiC substrate at the interface with the help of the thermal activation. As discussed for Ni-SiC system, such kind of defect decreases the stability of the SiC, leading to the more weakened Si-C covalent bonds adjacent to the metal layer compared to Ta/SiC system. The decomposition of SiC is therefore easier at 650^{o}C, accelerating the reactions between the Ta and SiC.

For the sample annealed at 800^{o}C (Fig. 17c), the reaction between Ta and SiC proceeds further to form Ta_2C and Ta_5Si_3:C in the inner part. The increase in C concentration next to the interface implies the possible formation of TaC, although this is not the dominant carbide. The adjacent increase in Ni and Si concentrations suggests the presence of Ni silicide.

A well-defined layer structure is formed at 950°C as shown in Fig. 17d. This high temperature is required for outwards Si diffusion and subsequent initiation of the reaction with both Ni and Ta to form the top TaNiSi layer. This layer probably also has embedded Ta_2C, Ta_5S_3:C and α-Ta_5Si_3. A thin Ni-rich layer is observed close to the coating/substrate interface, probably corresponding to the Ni_2Si phase. The intermediate region between these two layers is composed of TaC. The layered structure can be attributed to the requirement of minimization of the interfacial energy. It has been found that annealing a Ta-Ni alloy on a Si substrate results in $TaSi_2$ phase in the outer region and Ni silicide in the inner region next to the Si (Hung et al., 1986). Annealing amorphous Ni-Ta alloy film on GaAs (Lahav et al., 1987) leads to similar phase separation with an upper region of Ta(Ni)As and an inner region of NiGa. The common factor in these two systems is the layer structure with near-noble metal Ni compounds in contact with the substrate and refractory metal Ta compounds in the outer region. It appears that the sample heated at 950^{o}C has this trend of phase separation. Whether the top TaNiSi disappears or not and how the binary Ni or Ta compounds evolve progressively upon further annealing is of interest.

In the Ta/SiC system, the C atoms move faster than Si outwards through the coated layer and also react more readily with the deposited Ta. The total C content was higher than that of Si in the reaction product when the temperature is at or above 650^{o}C, indicating the formation of C deficiency region in the near interface side of the SiC. It has been proposed that the transition of Schottky to ohmic contacts during high temperature annealing is due to the creation of sufficient C vacancies in the near interface region of the SiC (Han et al., 2002; Nikitina et al., 2005). The C vacancies then act as donors to increase the net concentration of electrons and thus change the electrical properties of the SiC in the near surface region, resulting in the formation of ohmic contact. However, rectifying behaviour at 650°C (Cao et al., 2007^{b}) suggests that this mechanism is doubtful since plenty of C vacancies have formed at this temperature. Furthermore, rather deep ionization energy level of 0.51 eV (Aboelfotoh & Doyle, 1999) makes the carbon vacancy mechanism questionable as well. Instead of simple isolated C vacancies, more complicated defect configuration might be responsible for the formation of ohmic contacts.

4. Conclusion remarks

In the Ni/SiC system, 1) The formation of textured Ni_2Si via the reaction Ni + SiC = Ni_2Si + C consists of initial reaction-rate and subsequent diffusion controlled stages. The Ni_2Si islands are present for ultra thin initial Ni layer. The silicides formed at the interface depend on the Ni layer thickness and substrate surface condition. 2) The C released owing to the Ni_2Si formation reaction forms a thin graphite layer on the top of the surface and also tends to form clusters inside the reaction layer. The overall degree of graphitisation is higher at higher temperatures. 3) For the annealed Ni/SiC samples, argon ion etching before Ni deposition helps the formation of the multi-layer structure with less C agglomerated at the surface due to the quicker formation of the silicide Ni_2Si.

In Ta (or Ni/Ta)/SiC system, both silicides and carbides are formed after annealing. The reaction zone consists of a layered structure. A carbon deficiency region is preferentially produced in the near interface region of the underlying SiC. Amorphous Ni-Ta can be formed in Ni/Ta/SiC by the solid-state interfacial reaction. The existence of Ni lowers the formation temperature of carbide and silicide containing Ta, promoting the reaction between Ta and SiC. Although the sample heated at 950^{o}C showed the trend of phase separation. Whether the top TaNiSi disappears or not and how the binary Ni or Ta compounds evolve progressively upon further annealing in Ni/Ta/SiC is of further interest.

The carbon vacancy mechanism is likely to be questionable for the transition of Schottky to ohmic contacts during high temperature annealing. However, the sufficient alteration of the SiC subsurface with more complicated defect configuration by the reaction is important to the formation of the ohmic contact. Detailed investigation related to this issue is interesting.

5. References

Abe, K.; Sumitomo, M.; Sumi, T.; Eryu, O. & Nakashima, K.(2002). *Mater. Sci. Forum,* 389-393, 909-912.

Aboelfotoh, M. O. & Doyle, J. P. (1999). *Phys. Rev.,* B59, 10823–10829.

Adachi, S. (2004): in: *Handbook on Physical Properties of Semiconductors*, vol. 1, 269, Norwell, Kluwer Academic Publishers.

Backhaus-Ricoult, M. (1992). Acta Metal. Mater., 40, s95-103.

Berthod, P.; Aranda, L.; Vébert, C. & Michon, S. (2004). *Computer Coupling of Phase Diagrams and Thermochemistry*, 28, 159-166.

Bhanumurthy, K. & Schmid-Fetzer, R. (2001). *Composites,* A32, 569-574.

Brewer, L. & Krikorian, O. (1956). J. Electrochem. Soc., 103, 38-51.

Bächli, A.; Nicolet, M.-A.; Baud, L.; Jaussaud, C.& Madar, R. (1998). Mater. Sci. Eng., B56, 11-23.

Cao, Y.; Nyborg, L; Jelvestam, U. & Yi, D. (2005). *Appl. Surf. Sci.,* 241, 392–402.

Cao, Y.; Nyborg, L.; Yi, D. & Jelvestam, U. (2006). Mater. Sci.& Techno., 22, 1227-1234.

Cao, Y.; Nyborg, L. (2006). *Surf. Interface Anal*., 38, 748–751.

Cao, Y., Pérez-García, S.A. & Nyborg, L. (2007)[a]. *Mater. Sci. Forum,* 556-55, 713-716.

Cao, Y., Pérez-García, S.A. & Nyborg, L. (2007)[b]. *Appl. Surf. Sci.,* 254, 139–142.

Cao, Y.; Nyborg. L. & Jelvestam U. (2009). *Interface Anal.,* 41, 471–483.

Chen, J.S.; Kolawa, E.; Nicolet, M.-A. Ruiz, R.P.; Baud, L.; Jaussaud, C. & Madar, R. (1994). *J. Appl. Phys.*, 76, 2169-2175.
Chen, S.H.; Zheng, L.R.; Carter, C.B. & Mayer, J.W. (1985). *J. Appl. Phys.,* 57, 258-263.
Chou, T.C.; Joshi, A. & Wadsworth, J. (1990). *J. Vac. Sci. Technol,* A9, 1525-1534.
Ciccariello, J.C.; Poize, S. & Gas, P. (1990). *J. Appl. Phys.*, 67, 3315-3322.
Colgan, E.G.; Gambino, J.P.; Hong & Q.Z. (1996). *Mater. Sci. Eng.*, R16, 43-96.
d'Heurle, C.L.F.M. & Zhang, S.-L (2007). Silicides, In: *Handbook of Semiconductor Manufacturing Technology*, Doering, R; Nishi, Y (Ed.), p10-1 - 10-52, Taylor & Francis Group, LLC, ISBN 978-1-5744-4675-3, Boca Raton.
Fedorov, V.V.; Yedneral, A.F., Kachalov, V.M. & Borisov, V.T. (1986). *Phys. Met. Metall.,* 62, 96-99.
Feng, J.C.; Naka, M. & Schuster, J.C. (1997). *J. Mater. Sci. Lett.,* 16, 1116-1117.
Gambino, J.P. & Colgan, E.G. (1998). Silicides and ohmic contacts. In *Material Chemistry and Physics*, 52, 99-146.
Gasser, S.M.; Bächli, A.; Garland, C.M.; Kolawa, E. & Nicolet, M.-A.(1997). *Microelectronic Engineering*, 37/38, 529-534.
Geib, K.M.; Wilson, C.; Long, R.G. & Wilmsen, C.W. (1990). *J. Appl. Phys.*, 68, 2796-2800.
Guziewicz, M.; Piotroowska, A. Kaminska, Grasza, E. K.; Diduszko, R. Stonert, A. Turos, A.; Sochacki, M. & Szmidt, J. (2006). *Mater. Sci. Eng.,* B135, 289-293.
Han, S.Y. & Lee, J.-L. (2002). J. Electrochem. Soc., 149, G189-193.
Han, S.Y.; Kim, N.-K.; Kim, E.-D. & Lee, J.-L. (2002). *Mater. Sci. Forum,* 389-393, 897-900.
Han, S.Y.; Shin, J.-Y.; Lee, B.-T. & Lee. J.-L. (2002). *J. Vac. Sci. Technol.,* B20, 1496-1500.
Hollanders, M.A.; Duterloo, C.G.; Thijsse, B.J. & Mittemeijer, E.J. (1991). *J. Mater. Res.,* 6, 1862-1873.
Hsu, J.Y. & Liang, J.H. (2005). *Nucl. Instrum. Methods Phys. Res.,* B 241, 543–547.
Hung, L. S.; Saris, F. W.; Wang, S. Q. & Mayer, J. W. (1986). *J. Appl. Phys.,* 59, 2416.
Hähnel, A. & Woltersdorf, J. (2004). *Mater. Chem. Phys.,* 83, 380-388.
Kestle, A.; Wilks, S.P.; Dunstan, P.R.; Pritchard, M.; Pope, G.; Koh, A. & Mawby, P.A. (2000). *Mater. Sci. Forum,* 338-342, 1025-1028.
Kurimoto, E. & Harima, H. (2002). *J. Appl. Phys.*, 91, 10215-10217.
Iwaya, M.; Kasugai, H.; Kawashima, T.; Iida, K.; Honshio, A.; Miyake, Y.; Kamiyama, S.; Amano, H. & Akasaki, I. (2006). *Thin Solid Films,* 515, 768-770.
Jang, T.; Porter, L.M.; Rutsch, G.W.M. & Odekirk, B. (1999). *Appl. Phys. Lett.,* 75, 3956-3958.
Lahav, A.; Eizenberg, M. & Komen, Y. (1987). *J. Appl. Phys.,* 62, 1768.
Laurila, T.; Zeng, K. & Kivilahti, J.K. (2002). *J. Appl. Phys.,* 91, 5391-5399.
La Via, F.; Roccaforte, F.; Makhtari, A.; Raineri, V.; Musumeci, P. & Calcagno, L. (2002). *Microelectron. Eng.,* 60, 269-282.
La Via, F.; Roccaforte, F.; Raineri, V.; Mauceri, M.; Ruggiero, A.; Musumeci, P.; Calcagno, L; Castaldini, A. & Cavallini, A. (2003). *Microelectron. Eng.,* 2003, 70, 519-523.
Lavoie, C; Detavernier, C. & Besser, P. (2004). Nickel silicide Technology, In *Silicide Technology for Integrated Circuits*, Chen, Lih J. (Ed.), IEEE, London.
Le Claire, A.D. (1999). Diffusion in solid metals and Alloys, in *Numerical Data and Functional Relationships in Science and Technology,* Mehrer, H. (Ed.), III/26, Springer, 478.
Lee, P.S.; Mangelinck, D.; Pey, K.L.; Ding, J.; Dai, J.Y.; Ho, C.S. & See, A. (2000). *Microelectr. Eng.*, 51-52, 583-594.
Lee, P.-Y.; Yang, J.-L.; Lin, C.-K.& Lin, H.-M. (1997). *Metall. Mater. Trans.,* 28A, 1429-1435.
Lee, W.; Lee, J.; Bae, J.D.; Byun, C.S. & Kim, D.K. (2001). *Scripta Mater.,* 44, 97-103.

Lim, C.S.; Nickel, H; Naoumidis, A. & Gyarmati, E. (1997). *J. Mater.Sci.,* 32, 6567-6572.
Litvinov, V.L.; Demakov, K.D.; Agueev, O.A.; Svetlichnyi, A.M.; Konakova, R.V.; Lytvyn, P.M. & Milenin, V.V.(2002). *Mater. Sci. Forum,* 389-393, 905-908.
Liu, B.X. & Zhang, Z.J. (1994). Phys. Rev. B, 49, 12519-12527.
Lou, D.C., Akselsen, O.M., Solberg, J.K., Onsoien, M.I.; Berget, J. & Dahl, N. (2006). *Surf. Coatings Technol.,* 200, 3582-3589.
Lu, W.; Mitchel, W.C.; Landis, G.R.; Crenshaw, T.R. & Eugene Collins, W. (2003). *Solid-State Electron.,* 47, 2001-2010.
Lu, X.D. & Wang, H.M. (2004). *Acta Mater.,* 52, 5419-5426.
Madsen, L.D.; Svedberg,E.B.; Radamson, H.H.; Hallin, C.; Hjörvarsson, B.; Cabral, Jr., C.; Jordan-Sweet, J.L. & Lavoie, C.(1998). *Mater. Sci. Forum*, 264-268, 799-804.
Marinova, Ts.; Krastev, V.; Hallin, C.; Yakimova, R. & Janzén, E.(1996). *Appl. Surf. Sci.*, 99, 119-125.
Marinova, Ts.; Kakanakova-Georgieva, A.; Krastev, V.; Kakanakov, R.; Neshev, M.; Kassamakova, L.; Noblanc, O.; Arnodo, C.; Cassette, S.; Brylinski, C.; Pecz, B.; Radnoczi, G. & Vincze, Gy. (1997). *Mater. Sci. Eng.*, B46, 223-226.
Matzke, Hj. & Rondinella. V.V.(1999). in *Landolt Börnnstein. Added t.p.:Numerical Data and Functional Relationships in Science and Technology,* Beke, D.L. (Ed.), vol. III/33B1, 5-5, 6, Berlin, Springer.
Nash, P. & Nash, A. (1992). Alloy Phase Diagrams, In *ASM Handbooks*, Baker, H. (Ed.), Vol. 3, p2859-2860, ASM International, Materials Park, Ohio.
Nikitina, I.P.; Vassilevski, K.V.; Wright, N.G.; Horsfall, A.B. & O'Neill, A.G. (2005*). J. Appl. Phys.,* 97, 083709.
Ohi,A; Labis, J.; Morikawa, Y.; Fujiki, T.; Hirai, M.; Kusaka, M.& Iwami M.(2002). *Appl. Surf. Sci.,* 190, 366-370.
Olowolafe, J.O.; Solomon, J.S.; Mitchel, W. & Lampert, W.V. (2005). *Thin Solid Films*, 479, 59-63.
Ottaviani, G. (1979). *J. Vac. Sci. Technol.* 16, 1112-1119.
Park, J.S.; Landry, K. & Perepezko, J.H. (1999). *Mater. Sci. Eng.,* A259, 279-286.
Roccaforte, F.; La Via, F.; Raineri, V.; Calcagno, L. & Musumeci. P. *Appl. Surf. Sci.,* 2001, 184, 295-298.
Rodriguez, N.M.; Anderson, P.E.; Wootsch, A.; Wild, U.; Schlögl, R. & Paál, Z. (2001). *Journal of Catalysis,* 197, 365-377.
Sarkar, D.K.; Falke, M.; Giesler, H.; Teichert, S.; Beddies G. & Hinneberg, H.–J. (2000). *Appl. Phys.,* A70, 681-684.
Schuster, Julius C. (1993-1994). *Int. J. of Refractory Metals & Hard Materials,* 173-177.
Shifler, D.A. High-Temperature Gaseous Corrosion Testing, in *Corrosion: Fundamentals, Testing, and Protection, ASM Handbook,* Vol 13A, ASM International, 2003, p 650–681.
Smithells, C.J. (1967). Metals Reference book, vol. 2, 664, London, Butterworth & Co. Ltd.
Su, Y-K.; Chiou, Y-Z.; Chang, C-S.; Chang, S-J.; Lin, Y-C. & Chen, J. F. (2002). *Solid-State Electron.*, 46, 2237-2240.
Yoon, J-K; Byun, J-Y; Kim, G-H; Lee, J-K; Yoon, H-S & Hong, K-T. (2003). *Surf. Coating Technol.*, 168, 241-248.
Yuryeva, E.I. & Ivanovskii, A.L. (2002). *Russ. J. Coord. Chem.,* 28, 881-888.
Zhang, Q.; Lai,W. S. & Liu, B. X. (2000). Phys. Rev., B 61, 9345–9355.
Zheng, L.R.; Hung, L.S. & Mayer, J.W. (1983). *J. Vac. Sci. Technol.*, A1, 758-761.

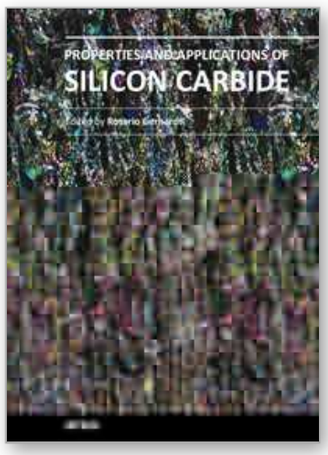

Properties and Applications of Silicon Carbide
Edited by Prof. Rosario Gerhardt

ISBN 978-953-307-201-2
Hard cover, 536 pages
Publisher InTech
Published online 04, April, 2011
Published in print edition April, 2011

In this book, we explore an eclectic mix of articles that highlight some new potential applications of SiC and different ways to achieve specific properties. Some articles describe well-established processing methods, while others highlight phase equilibria or machining methods. A resurgence of interest in the structural arena is evident, while new ways to utilize the interesting electromagnetic properties of SiC continue to increase.

InTech Europe
University Campus STeP Ri
Slavka Krautzeka 83/A
51000 Rijeka, Croatia
Phone: +385 (51) 770 447
Fax: +385 (51) 686 166
www.intechopen.com

InTech China
Unit 405, Office Block, Hotel Equatorial Shanghai
No.65, Yan An Road (West), Shanghai, 200040, China
中国上海市延安西路65号上海国际贵都大饭店办公楼405单元
Phone: +86-21-62489820
Fax: +86-21-62489821

IntechOpen